

Chapter 3

Dynamics of the Transient Intermediate during SRP-SR Association

A version of this chapter has been prepared for submission.

3.1 Abstract

Interactions between proteins are in the center of biology. Kinetic studies of protein-protein interaction have proposed a mechanism in which proteins initially form a pre-equilibrium transient intermediate along the association pathway that subsequently relaxes to the stable complex. However, the landscape of the transient intermediate that precedes formation of the stable complex is still not well defined experimentally. In this work, we directly visualized the conformational dynamics of the early complex as a transient intermediate during the assembly between two GTPases in the signal recognition particle (SRP) and its receptor (SR) under equilibrium condition. We show that the interaction surface of the early complex shares both similarities and differences with that of the stable complex. In addition, a broad conformational distribution of the early complex allows the free proteins to search optimal routes in the configuration space toward to an efficient stable complex assembly. Interestingly, the dynamics of the early complex actively responds to the external biological cues that the SRP-SR interaction dictates. Collectively, understanding the landscape of the SRP-SR early complex provides a general feature that is shared by the transient intermediate during protein assembly.

3.2 Introduction

Most proteins rely on interacting with one another to carry out their biological functions (1, 53-56). However, unbound proteins often need to change their conformation substantially to form stable complexes. A model that combines both the “induced fit” and the “conformational selection” hypotheses postulates three steps

for the protein-assembly process (57-59). The initial step arises from a diffusing binding event between proteins form a transient intermediate in solution; subsequently, the complementary structures are recognized and selected from the conformational ensemble of the transient intermediate; and last, the intermediates composed of complementary structures reorient into a native, stable complex with a fitted interaction surface. In this model, formation of the transient intermediate is mostly mediated by nonspecific collisions and directional long-range electrostatic interactions; and does not undergo extensive conformational rearrangements in proteins. Although nonspecific and weak, a transient intermediate could give rise to the rate of complex formation because proteins that are loosely held in this intermediate are given time to undergo rearrangements and reorientations to form short-range interactions that are required for the interaction surface of a stable complex.

Despite significant progresses in understanding how the transient intermediate kinetically facilitates the protein assembly (60), direct visualization on the transient intermediate during protein assembly pathway is still much less common. Several studies were reported to visualize the dynamics of the transient encounter complexes that are formed upon collision, but these encounter complexes do not lead to the formation of stable complexes (61, 62). During assembly of a stable complex, the transient intermediate is much more unstable than the stable complex, so it either rearranges into a stable complex or dissociates rapidly. Only a very small population of the intermediate can be captured in an ensemble experiment, and this situation complicates the structural study of the transient intermediate. To understand the conformational dynamics of the

transient intermediate during protein assembly, we choose the interaction between two guanosine triphosphatases (GTPases) in the signal recognition particle (SRP) and the SRP receptor (SR) as a model system because the transient intermediate during the SRP-SR assembly process can be isolated and characterized under equilibrium condition (4, 5).

3.2 Results

SRP and SR GTPases initially associate with one another to form an unstable, transient intermediate named early complex (step 1 in figure 3.1A), and then the early complex undergoes extensive local conformational rearrangements to form the stable complex (step 2 in figure 3.1A). Interestingly, the conformational rearrangements to form the stable complex are largely dependent on the γ -phosphate of the guanosine triphosphate (GTP) molecules that bound to both GTPases. If binding guanosine diphosphate (GDP) instead of GTP, the SRP•SR complex is stalled at the stage of the early complex without further rearranging into the stable complex (figure 3.1A). Taking the advantage of this distinct feature, we could generate an ensemble of early complex by stopping it forming the stable complex. Thus the structural properties of the early complex can be directly characterized in detail under equilibrium condition. In the following experiment, the early complex is formed using GDP; and the stable complex is formed with non-hydrolyzable GTP analogue, 5'-guanylylimido-diphosphate (GMPPNP).

Formation of the transient intermediate is mainly guided by long-range electrostatic interactions and nonspecific collisions within solvent cages; therefore, it is believed that

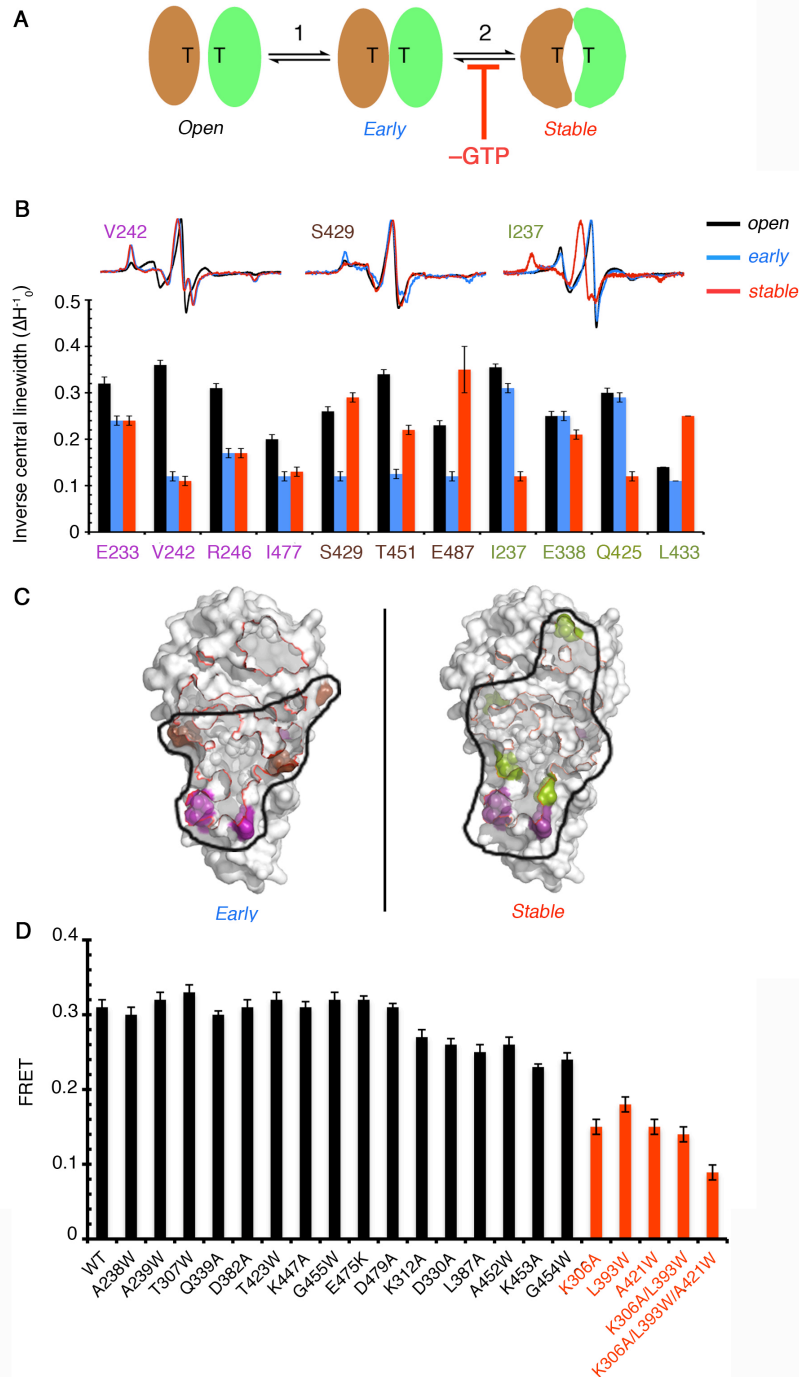


Figure 3.1. The interface of the SRP-SR early complex is both similar to and different from that of the stable complex. **(A)** Schematic mechanism of SRP-SR assembly. Upon directional collision, SRP and SR form a non-specific early complex (step 1), which serves as a transient intermediate that leads to the formation of a stable, specific complex (step 2). Removing GTP from the solution stalls the early complex from evolving into the stable complex. Brown and green denote for SRP and SR, respectively. T denotes GTP. **(B)** The mobility of residues changed upon the formation of either the early complex

(brown), the stable complex (green), or both (purple). (C) Interaction surface of the early and stable complexes mapped by EPR measurements. (D) Mutations that disrupt the formation of the stable complex do not significantly affect the thermodynamic stability of the early complex. Mutations causing moderate defect in the formation of the early complex are highlighted in red.

very few short-range interactions can be made in the intermediate (63). The questions arose are what the interaction surface of the transient intermediate looks like and how different it is from that of the stable complex. To answer these questions, we explored the interaction surface of both the early and stable SRP•SR complexes using electron paramagnetic resonance (EPR) spectroscopy. The strategy was to select the residues to examine whether their mobility was affected by the formation of either the early or the stable complexes. These residues were replaced by cysteines for site-directed spin labeling with nitroxide probe (1-oxy-2,2,5,5-tetramethyl-3-pyrrolyl-3-methyl) methanethiosulfonate (MTSSL). Sites that the nitroxide probe modification does not affect the ability of SR to interact with SRP are selected for EPR measurements. For each individual residue, EPR measurement was carried out to characterize the mobility of the spin-label in the apo-SR (figure 3.1B, black), the early complex (figure 3.1B, blue), or the stable complex (figure 3.1B, red). From the line width of the central resonance and the overall breadth of the spectra along the magnetic field axis, we could derive a qualitative description of the local mobility of the nitroxide probe-labeled SR. If the mobility of the spin label decreases upon complex formation, then the labeled residue is considered to be involved in strong interactions that contribute to form the interface of this complex.

Shown in figure 3.1B, three classes of residues were identified from the EPR measurements. The first class includes four residues that are represented by residue 242

(figure 3.1B and figure 3.S1, purple), in which the apo-SR exhibits restrained EPR spectra with a majority of molecules being mobile. Upon formation of both the early and stable complexes, decreased mobility of the nitroxide probes indicated that these residues were involved in local interactions, suggesting that these residues are engaged in the interface of both complexes. We also identified residues that are involved in the formation of interfaces of either the early complex (figure 3.1B and figure3.S1, brown) or the stable complex (figure 3.1B and figure3.S1, green). In either group, mobility of these residues was only affected by the interaction surface of one conformational state but not the other. Summarizing the above results, we were able to obtain a collective view of the interaction surfaces the early (figure 3.1C, left panel) and stable complexes (figure 3.1C, right panel). In the early complex, most contacts between SRP and SR were concentrated in the N/G domain interface and the N domain, whereas most of the G domain made little contribution to the interaction surface. In contrast, the interface of the stable complex covered both G and N domains, consistent to the interaction surface that was shown in the co-crystal structure of SRP-SR stable complex (red line on surface representation in figure 3.1C) (20). Taken together, EPR measurements suggested that the early complex did contain a detectable interaction surface that shared both similarities and differences to that of the stable complex (figure 3.1C).

Based on the above observation, we reasoned that the fact that the early and stable complexes share a common interaction surface would allow us to mutate residues to disrupt the formation of both complexes. To this end, we introduced 24 mutations to the SR protein, and all of them severely blocked the formation of the stable complex (figure 3.1D and figure3.S2B) (9). The stability of early complex formed with SR mutants was

measured using fluorescence resonance energy transfer (FRET) between coumarin (DACM) labeled SRP C235 and BODIPY-fluorescein (BODIPY-FL) labeled FtsY C487 (4). Whether a mutation was defective in forming the early complex could be derived from the extent of reduction in FRET efficiency compared to that of the wild-type SR at a fixed protein concentration. To our surprise, most of the mutations did not disrupt the formation of the early complex at protein concentrations that we tested (black bars in figure 3.1D). Only three mutations caused moderate reduction in the stability of the early complex by a factor of up to four (red in figure 3.1D and figure3.S2A). A triple mutation including all three positions further destabilized the early complex by only a factor of eight (red in figure 3.1D and figure3.S2A).

The mutagenesis experiments showed that mutations severely disrupting the formation of the stable complex were only marginally defective in forming the early complex, suggesting that these two complexes employed distinct interaction surfaces. This conclusion was seemingly contradictory to what was suggested by the EPR measurements. We then speculated that the early complex did not contain a defined interface like the stable complex did. If the early complex was composed of multiple distributions of conformations and each of them used different interface from one another, then mutations that only disrupted the interface of particular conformations would not affect other conformations that were still bound to maintain the stability of the early complex. In contrast, the stable complex could contain only a few well-defined conformations so mutations that disturbed one population would substantially reduce the stability of the complex.

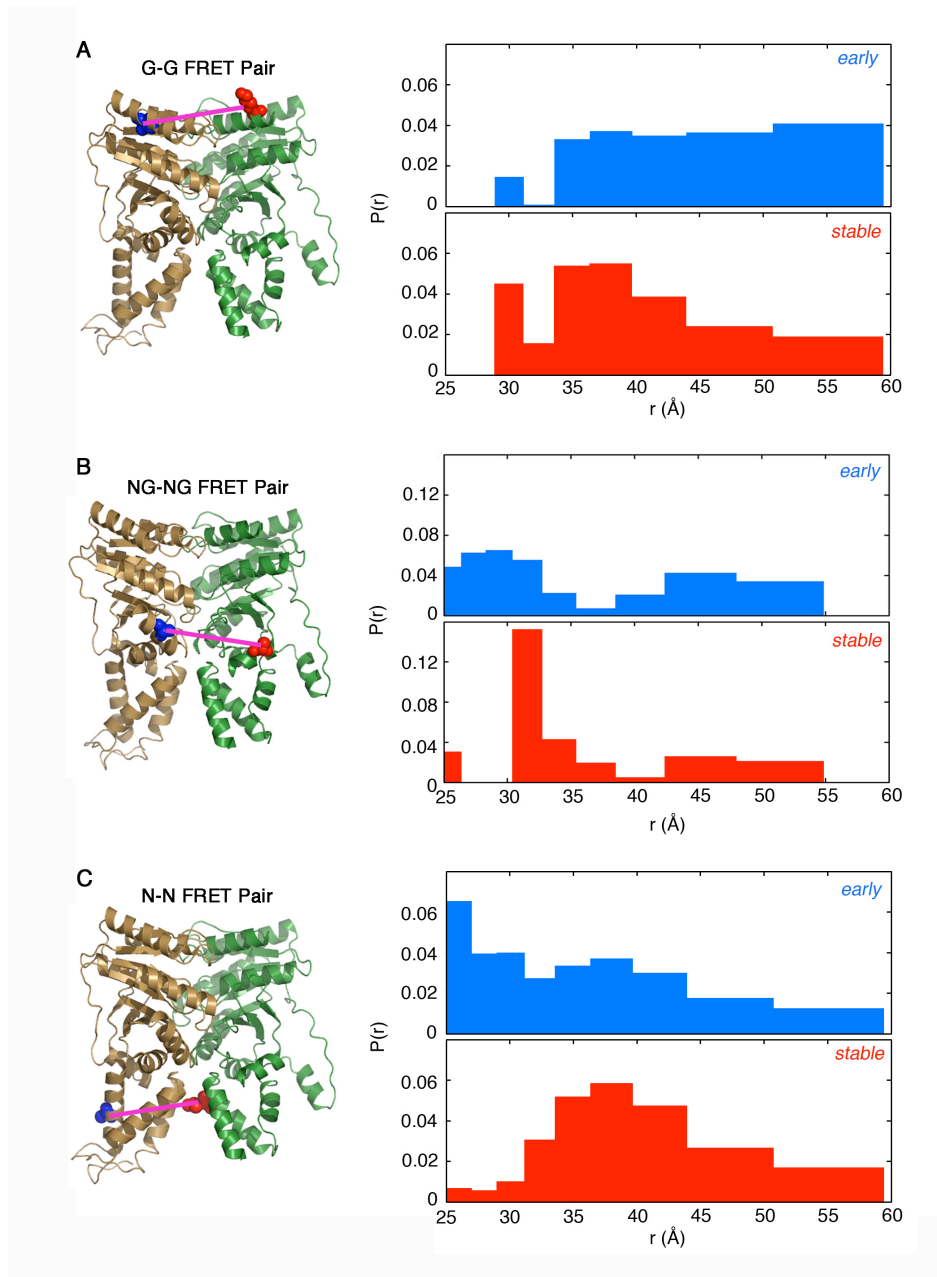


Figure 3.2. The early complex has a more broad conformational distribution than the stable complex. Fluorescence decay kinetics of the donor fluorophore (blue) was measured in the presence of the acceptor fluorophore (red). Distributions of $P(r)$ were derived from the maximal entropy analyses of the TR-FRET kinetics data. Left panel in (A), (B), and (C) shows position of the G-G, NG-NG, and N-N FRET pairs, respectively. Distribution of $P(r)$ was measured for each FRET pair in the pre-formed early complexes (blue) or stable complexes (red) under equilibrium condition. Gold and green proteins are SRP and SR GTPases, respectively.

To test this hypothesis, we carried out time-resolved FRET experiments to measure the distance distribution between a fluorescence donor (DACM) on SRP and an energy acceptor (BODIPY-FL) on SR in an ensemble of the SRP•SR complexes. These measurements provide nanosecond snapshots of donor-acceptor distance distributions of either the early or the stable complex (figure 3.S3) (64). Three different positions were selected to measure distance distributions between the G domains (G-G, figure 3.2A), the NG domain interfaces (NG-NG, figure 3.2B), and the N domains (N-N, figure 3.2C) of both proteins. For all three pairs, the early complex generated more broad distance distributions than the stable complex (figure 3.3 and figure 3.S4, blue vs red). In addition, it is notable that the conformational distribution in the stable complex already existed in the early complex, suggesting that the molecular ensemble of the early complex underwent the conformational sampling to form the stable complex. These observations support the hypothesis that the early complex comprises more conformational populations than the stable complex.

Further, the observed pattern of distance distribution also revealed the process of the early complex assembly. Distance as short as ~ 25 Å was observed for the N-N pair, while the G-G pair generated a ubiquitous distance distribution that had no dominating peaks. This pattern of distance distributions suggested that the formation of the early complex initiated from the close contacts between N-domains of both proteins. We reasoned that these contacts could be originated from the long-range electrostatic interactions that commonly facilitate the formation of an encounter complex. Thus, we calculated the electrostatic surface of the GTPase domains of both the SRP and SR using adaptive Poisson-Boltzmann solver (APBS) (65). The N domain of the SRP contains a

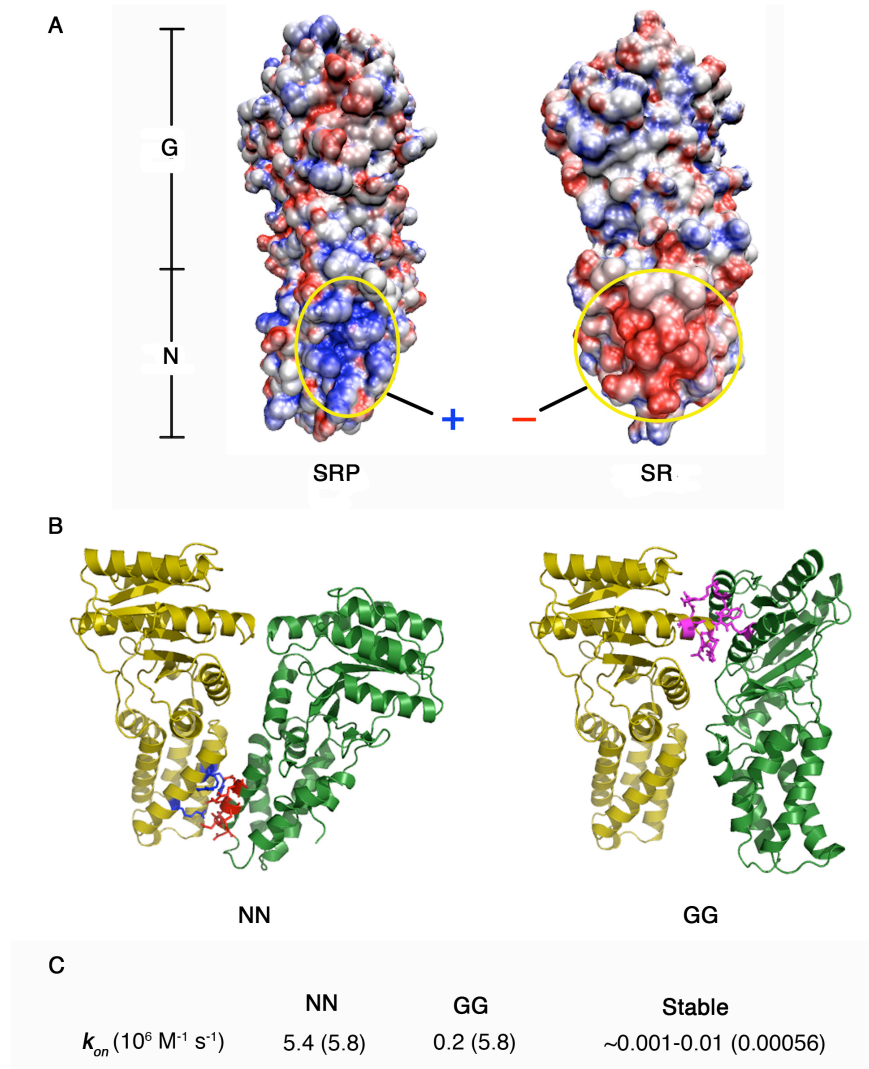


Figure 3.3. The long-range electrostatic interaction between sites with complementary charges drives the formation of the early complex. **(A)** Sites in the N domains of the SRP and SR GTPases contained complementary charges. Blue and red denotes positive and negative charges, respectively. **(B)** Molecular docking simulation generated two groups of conformations (NN and GG) that accounted for the ensemble of the early complex. Gold and green proteins are SRP and SR GTPases, respectively. In the NN conformations, hot spots analyses predicted that the positive residues on the SRP (blue) contacted the negative residues on the SR (red) via electrostatic interaction. In the GG conformations, hot spots analyses predicted that that van der Waals interaction between residues (pink) on the G domains contributed to the formation of the interface. **(C)** Association rate constants derived from the Brownian dynamics calculation were comparable to the experimental measured rate constants (in parentheses).

positively charged patch, whereas that of the SR has complementary negative charges (figure 3.3A). Thus, a general non-specific electrostatic interaction between these two patches could facilitate the assembly of the early complex.

To provide a molecular picture of the early complex, we carried out molecular docking simulation; and the first two highest-ranked groups, denoted as NN and GG, were selected to describe the possible conformations of the early complex (figure 3.3B and figure3.S5). Conformers in the NN group placed N domains of both GTPases adjacent to each other whereas the G domains were apart; and the interface of the NN complexes was consistent to what was identified by EPR spectroscopy (figure 3.1C, left panel). Interestingly, the contact sites in the N domains were composed of the residues bearing complementary charges as identified in APBS calculation, suggesting that the formation of the NN complexes was primarily mediated by a general electrostatic interaction (figure 3.3B, blue and red residues in the left panel). In contrast to the NN group, the GG group contained complexes with G domains contacting one another but N domains being separated; and the interface of the GG complexes were mainly mediated by van del Waals interaction between residues in G domains (figure 3.3B, pink residues in the right panel). As one means to validate the reliability of the docking simulation, we examined the distance distribution between all three FRET pairs using the complexes generated in these two groups. Both groups were needed to produce the distance distributions that were qualitatively comparable to the experimental measurements (figure 3.S7 vs figure3.2, blue), suggesting that both the NN and GG conformations existed as possible conformational states of the early complex. In addition, we also collected evidence suggesting that the NN complexes were more likely to be the

dominant population in the early complex under the equilibrium condition. First, residues that were affected in the EPR measurements resided in the interfaces of complexes in both groups but primarily the NN group (figure 3.S6). Second, the theoretically estimated associate rate constants for early complex formation based on the NN complexes agreed well to what were measured experimentally, whereas, the GG complexes produced the association rate constant that was slower than the experimental value by a factor of thirty (figure 3.3C).

We next ask whether the conformational dynamics of the SRP-SR early complex responds to the biological cue that it dictates. Since the interaction between the SRP and SR GTPases regulates the co-translational protein targeting process, we speculated that the cargos for SRP could alter the dynamics of the early complex. To this end, we measured the conformational distribution of the early complex in the presence of an authentic SRP cargo, RNC_{FtsQ} , a translating ribosome with the first 74 amino acids of the stalled FtsQ nascent chain (5). Early complex was incubated with RNC_{FtsQ} to form the early targeting complex; subsequently the TR-FRET experiment was carried out to obtain the distance distributions of three different FRET pairs. Notably, cargo substantially narrows the distance distribution of all measured FRET pairs. Instead of being broad, bipolar distance distributions of the early complex were observed in the presence of RNC_{FtsQ} (figure 3.4A and figure3.S8). These observations suggested that the cargo modulated the dynamics of the early complex into a limited configuration space in which the success rate of selecting complementary structures were increased, providing additional explanation to why cargos could kinetically accelerate the formation of the stable complex (5).

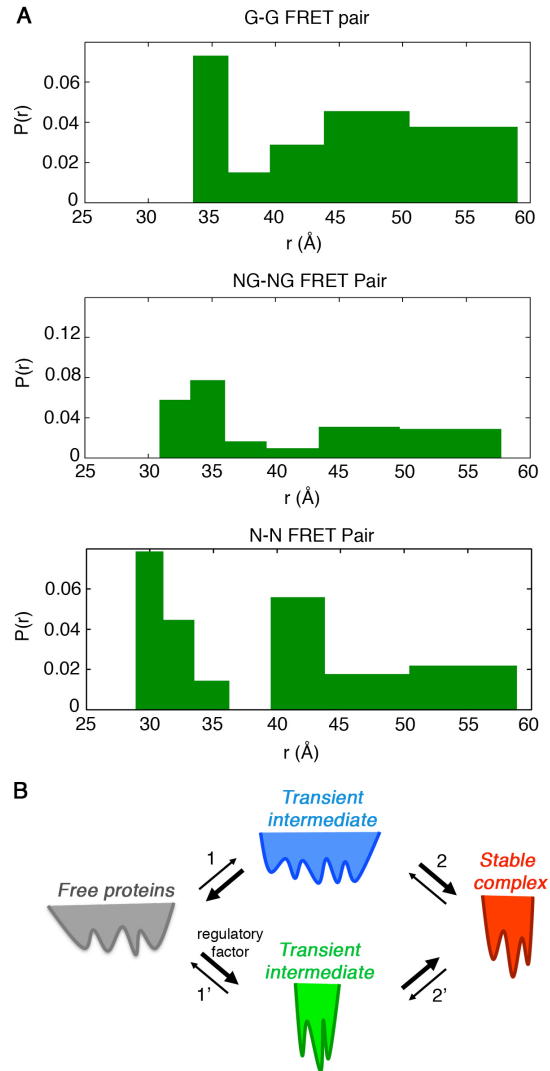


Figure 3.4. SRP-dependent cargo confined the conformational distribution of the early complex. **(A)** Distances between the FRET pairs were measured in a preformed early targeting complex in the presence of RNC_{FtsQ}. Distributions of $P(r)$ were extracted from the maximal entropy analyses of the TR-FRET kinetics data. **(B)** A schematic diagram of energy landscapes of the transient intermediate and stable complex during protein-protein assembly processes. The presence of an external factor changes the landscape of the transient intermediate to alter the thermodynamic and kinetic framework of the protein-protein assembly.

3.4 Discussion

Our work suggests that the ensemble of the early complex is a collection of various distinct conformational states (blue in figure 3.4B). In this ensemble, the early complex

samples through a broad range of the conformational space to seek optimal conformations that are efficient to produce short-range interactions for formation of the stable complex (step 2 in figure 3.4B), which contains a restrained conformational distribution (red in figure 3.4B). More importantly, the conformational distribution of the early complex could respond to the cargos that SRP needs to deliver via the SRP-SR interaction (step 1' and green in figure 3.4B), suggesting that the structural dynamics during protein-protein interactions could play a regulatory role to the biological processes that they dictates. The observed features of the SRP-SR early complex during the formation of the stable complex could represent general features that are shared by the transient intermediates during protein assembly.

The direct visualization of the transient intermediate during protein assembly adds to a growing collection of examples to support the notion that the intermediate contains a conformational ensemble in which the complementary structures are selected for further induced fit (figure 3.4B). The efficiency of the stable complex assembly is more affected by the possibility that the complementary structures are successfully selected than by the rate constants of the intermediate assembly (54). In addition, external regulatory factors can also affect the conformational landscape of the transient intermediate to alter the thermodynamic and kinetic framework of the protein assembly. Since the transient intermediate is possibly formed prior to the free proteins undergo conformational rearrangements; these conformational distributions could be well built in the innate conformational fluctuations of the free proteins (gray in figure 3.4B) (58). Upon formation of the transient intermediate, the conformational fluctuations in the free protein can be further reduced to expedite the formation of the stereospecific and stable complex.

This mechanism can be viewed as a funnel-shaped binding model in which many possible routes to approach the stable complex can be selected from the conformational distributions within the ensemble of the transient intermediate.

3.5 Materials and Methods

3.5.1 Materials

The *E. coli* SRP and SR GTPases (Ffh and FtsY, respectively), and 4.5S RNA were expressed and purified as described previously (4, 66). FtsY (47-497) was used in all the fluorescence and EPR measurements. The abilities of FtsY(47-497) to interact with SRP and respond to the cargo are similar to those of full length FtsY. Single cysteine mutants of Ffh and FtsY and stable complex defective mutants of FtsY were constructed using the QuickChange mutagenesis procedure (Stratagene). All mutants were expressed and purified using the same procedure as that for the wild-type proteins. Fluorescent dyes N-(7-dimethylamino-4-methylcoumarin-3-yl)maleimide (DACM) and BODIPY-FL-N-(2-aminoethyl)-maleimide were from Invitrogen.

3.5.1.1 RNC_{FtsQ} purification

Homogeneous RNC_{FtsQ} were generated from In vitro translation reactions using membrane free cell extract prepared from MRE600 cells, and RNC_{FtsQ} were purified through affinity chromatography and sucrose gradient centrifugation as described previously (5, 67). Purified RNC_{FtsQ} can serve as functional cargos in protein targeting reaction as they can bind SRP, trigger-factor, and secYEG translocon complex. In quantitative assays, purified RNC_{FtsQ} exhibit the same affinity for SRP as those measured with RNCs that do not contain an affinity tag (68).

3.5.1.2 Fluorescence labeling

For FRET measurements, DACM and BODIPY-FL were used to label single-cysteine mutants of Ffh and FtsY, respectively, as described previously (4). Labeled

protein was purified as described (4), and the efficiency of labeling was typically $\geq 95\%$ with a background of $< 5\%$.

3.5.1.3 Spin labeling

All single cysteine FtsY mutants, in 20 mM HEPES pH8.0 buffer with 150mM NaCl and 2mM EDTA, were incubated with 10 molar excess of dithiothreitol (DTT) at room temperature for 1-2 h to reduce any disulfide cross-linking. DTT was removed from protein by passing through gel filtration column. In the labeling reactions, a 3- to 5 fold molar excess of spin label (1-oxy-2,2,5,5-tetramethyl-3-pyrrolyl-3-methyl)methanethiosulfonate (MTSSL) (Toronto Research Chemicals, Toronto, Canada) was added to the argon degassed protein sample ($\sim 100 \mu\text{M}$). The spin-label reactions were carried out at room temperature in the dark for 2-3 h. Excess MTSSL was removed by gel filtration. The labeling efficiency was determined by EPR measurements using a TEMPO calibration curve (Bruker user manual). The typical efficiency of spin label is usually $> 80\%$; and a $< 5\%$ background labeling is observed with cysteine-less wild-type protein labeled following the same protocol. Only functional labeled FtsY mutants similar to wild-type enzymatic activity were used for subsequent EPR measurements.

3.5.2 Experimental strategy

In order to directly visualize the transient intermediate along the association pathway between SRP and SR, we used a combination of different techniques, including electronic paramagnetic resonance (EPR), steady-state FRET, mutagenesis, and time-resolved fluorescence energy transfer (TR-FET). EPR technique was used to explore the interaction surface of both the early and the stable complexes. Mutagenesis and steady-state FRET assay were used together to determine the equilibrium stability of the early

complex formed with different SR mutants. The TR-FET technique was used to directly measure the distance distribution between the donor molecule on SRP and acceptor molecule on SR. By collecting the distance distribution between donor and acceptor at different positions on both SRP and SR, we can characterize the conformational dynamics of the early and stable complexes in the configuration space. Taken together, these techniques enable us to directly characterize the structural dynamics of the early and stable complexes under equilibrium condition.

3.5.3 Electron paramagnetic resonance (EPR) measurements

EPR measurements were carried out to determine the local mobility of 9 spin label molecules in the form of apo-FtsY, the early complex or the stable complex. For FtsY in apo-form, 75-100 microM spin-labeled FtsY was used to obtain the EPR spectra. The early complex was formed by mixing 30 microM spin-labeled SR with 90 microM SRP in the presence of GDP. Based on the binding affinity of the early complex (K_d values of 4-10 μM) (4), more than 90% of labeled FtsY is in complex form with SRP in the state of the early complexes. The stable complex was formed by mixing 30 microM spin-labeled-SR with 60 microM SRP in the presence of the GTP analogue 5'-guanylylimido-diphosphate (GMPPNP). More than 99% of labeled FtsY is in complex form with SRP in the state of the closed complex according to the reported K_d values of the stable complex (~ 16 nM) (4).

EPR spectra were acquired with a 9.4 GHz (X-band) Bruker EMX EPR spectrometer equipped with an ER 4119HS cavity at 20-23 °C. In order to generate the local mobility of spin labels, 40% glycerol was added in all samples to eliminate the motion of protein global tumbling. Since the center line width (ΔH_0) of EPR spectra

stays the same at microwave powers of 0.2, 2, or 5 mW, all scans were carried out using microwave power of 5 mW to improve the signal-to-noise ratio. The modulation amplitude was set at 2 gauss and magnetic field sweep width was set as 100 gauss. For each sample, an averaged spectrum was obtained from approximately 32 to 64 scans and the background signal was subtracted.

During EPR measurements, the energy absorption process takes place when the unpaired electron in the probe transits from the ground state to the excited state. EPR signals can be observed when the scanning magnetic field is in resonance with the electron spin frequency, akin to the mechanism in nuclear magnetic resonance phenomenon. It has been shown that the center signal is sensitive to both the local environment and secondary structure. Thus we used the central line width (ΔH_0), which is measured from peak to peak of the center signal (figure 3.1B), as a way to characterize residue mobility. Collectively, the mobility measurements of a set of labeled residues can be used to describe dynamics of the interested area.

3.5.4 Steady-state fluorescence measurements

Our previous work showed that the rate constant of early complex formation is rapid and the K_d value of this complex is 4-10 μM . We therefore measured the relative equilibrium stability of the early complex formed by different SR mutations using the FRET assay at a steady-state condition. All measurements were carried out at 25 °C in assay buffer [50 mM KHEPES, pH 7.5, 150 mM KOAc, 2 mM $\text{Mg}(\text{OAc})_2$, 2 mM DTT, 0.01% Nikkol] on a Fluorolog-3-22 spectrofluorometer (Jobin Yvon, Edison, NJ). FRET measurements were carried out using an excitation wavelength of 380 nm and an emission wavelength of 470 nm. FRET efficiency was calculated as described.

To compare the relative equilibrium stability of the early complexes formed with different SR mutants, 4 or 20 microM acceptor labeled SR-mutants were incubated with 1 microM donor-labeled SRP in the absence of GTP or GTP analogue. Equilibrium is established upon manual mixing. FRET efficiency was calculated as described. For representative mutants, equilibrium titrations were carried out in the presence of a small, fixed amount of donor-labeled SRP and increasing amounts of acceptor-labeled SR in the absence of GTP or GTP analogues. FRET efficiency was plotted as a function of SR concentration ($[SR]$). The data were fit to Eq. (3.1),

$$E = E_1 \times \frac{[SR]}{K_d + [SR]} \quad (3.1)$$

in which E_1 is the FRET value (end point) when all the SRP are bound to SR, and K_d is the equilibrium dissociation constant of the early complex.

3.5.5 Time-resolved fluorescence energy transfer (TR-FET) measurements

TR-FET experiments were carried out to measure the distance distribution between the donor (DACM) on SRP and acceptor (BODIPY-FL) on SR. Donor-only measurement was carried out in the presence of 5 microM or 1 microM DACM-labeled SRP for the early and stable complexes, respectively. For the early complex, 5 microM DACM-labeled SRP and 50 microM BODIPY-FL-labeled SR were mixed together in the presence of GDP. For the stable complex, 1 microM DACM-labeled SRP and 8 microM BODIPY-FL-labeled SR were mixed in the presence of GMPPNP. Formation of both complexes was complete after a 20-minute incubation at room temperature at dark.

The time-resolved DACM fluorescence-decay kinetics measurements were carried out with a picosecond streak camera (C5680; Hamamatsu Photonics) in the photon-counting mode (69, 70). The excitation wavelength was set at 355 nm from a

third harmonic of a regeneratively amplified mode-locked Nd-YAG laser (pulsewidth is ~ 15 ps) (Vanguard, Spectra-Physics). A band-pass filter of 450 ± 5 nm was used as the emission filter. This filter is capable of minimizing the fluorescence from the acceptor (BODIPY-FL), and there was no observable fluorescence signal from either the buffer solution or the unlabeled protein. DACM fluorescence decay kinetics was measured in both short (5 ns) and long (20 ns) time scale, whose time resolutions are ~ 10 and ~ 40 ps, respectively.

3.5.6 Data fitting and analysis

The measured short and long timescale data were spliced together, and the combined traces were compressed logarithmically before fitting process (70 points per decade). The splicing and compression did not introduce artifact to the interpretation of data (64). The TR-FET data analysis can be described as a numerical inversion of a Laplace transform [$I(t) = \sum_k P(k) \exp^{-kt}$] (71, 72). In this work, two algorithms were used to invert the kinetics data with regularization methods that impose additional constraints on the properties of $P(k)$. The simplest constraint that applies to the FET kinetics data is the non-negativity constraint, $P(k) \geq 0$ ($\forall k$).

The first method is based on the least-squares fitting algorithm. The kinetics data were fitted using a MATLAB algorithm (LSQNONNEG) (Mathworks, Natick, MA) that minimizes the sum of the squared deviations (χ^2) between observed and calculated values of $I(t)$, subject to the non-negativity constraint. The LSQNONNES algorithm produces the narrowest $P(k)$ distributions and smallest values of χ^2 with relatively few nonzero components.

The second method is based on the maximum entropy theory. The information theory proposes that the least biased solution to the inversion problem is to minimize χ^2 and maximize the breadth of $P(k)$ (73). This regularization condition can be met by maximizing the Shannon-Jaynes entropy of the rate-constant distribution

$$\left\{ S = -\sum_k P(k) \ln[P(k)] \right\} \text{ with the satisfaction of the non-negativity constraint.}$$

Maximum-entropy (ME) fitting generates stable and reproducible numerical inversions of the kinetics data. The balance between χ^2 minimization and entropy maximization is evaluated by the L-curve analysis. This approach yields upper limits for the widths of $P(k)$ consistent with our experimental data. The $P(k)$ distributions from ME fitting are broader than those obtained with LSQNNPNEG fitting, but exhibit maxima in similar locations.

Both methods were used to generate the decay rate distribution $P(k)$.

Subsequently, a coordinate transformation using the Förster relation (Eq. 3.2) was carried out to convert the probability distribution of the decay rates k to the donor-acceptor distances r .

$$r = R_0 \left(\frac{k}{k_0} - 1 \right)^{1/6}. \quad (3.2)$$

This transformation produces the donor-acceptor distance distribution $P(r)$ from the decay rate distribution $P(k)$. The Förster critical length, R_0 , for the DACM/BODIPY-FL pair is $\sim 47 \text{ \AA}$. The value of k_0 was obtained from donor-only measurements. At distances larger than $1.5 R_0$, energy transfer quenching of donor-fluorophor cannot compete with the excited-state decay so the energy transfer does not take place efficiently. In addition, at distances $\sim 13 \text{ \AA}$, the Förster model does not reliably describe

FET kinetics. Therefore, our TR-FET measurements can provide information about donor-acceptor distances only in the range from 13 to 70 Å.

3.6.7 Theoretical simulation

3.5.7.1 Early complex docking

ClusPro 2.0 docking server was used for early complex docking. During the docking, *E. coli*-Ffh was set to a static receptor while *E. coli*-FtsY was set to a ligand that searched for the best docking position with the receptor. The initial docking positions were generated by the Fast Fourier Transform method and docking positions were clustered according to their root mean square deviations. Clusters were sorted via a filter that was set to an electrostatic-favored energy function. The ranking of the clusters was determined by the number of structures that each cluster contained. The top five clusters have 89, 88, 65, 59 and 46 structures, respectively. The top two clusters, named GG and NN, were chosen for further analyses.

3.5.7.2 Hot spots analyses

Knowledge-based FADE and Contacts (KFC) server was used for hot spots prediction for GG and NN structures. Only the central structures of GG and NN clusters were used for this analysis. The hot spots were predicted by either K-FADE model (based on shape specificity feature) or K-CON model (based on biochemical contacts). Both models were trained with a set of alanine-scan experimental data and hot spots were defined as $\Delta\Delta G$ larger than 2 kcal/mol.

3.5.7.3 Brownian dynamics

BrownDye was used for Brownian Dynamics calculations (74). APBS (Adaptive Poisson-Boltzmann Solver) was used to calculate the electrostatic potentials (65). Partial

atomic charges and atomic radii were assigned from the PARSE parameter set. The dielectric constants were assigned to be 4 in the protein interior and 78 in the exterior. Grids were assigned with dimensions of $193 \times 193 \times 193$ points. Temperature was set to 298 K and ionic strength was set to 100 mM. Brownian dynamics trajectories were started at a minimum intermolecular separation that still gave spherically symmetric forces. The number of trajectories to estimate the association rate varied from 40,000 to 100,000 depending on how fast the association rates were. The reaction criterion was specified by the atom-contact pairs that were defined by the structure of the complex. All the intermolecular nitrogen-oxygen pairs within 0.55 nm were considered as within the reaction criterion. A series of simulations with different levels of reaction criteria were generated by systematically tuning the required atom-contact number from 3 to 7. Three structures were used for this analysis to obtain the association rate constants: the central structure of GG cluster, the central structure of NN cluster and the stable complex from crystal structure.

3.6 Supplementary Figures

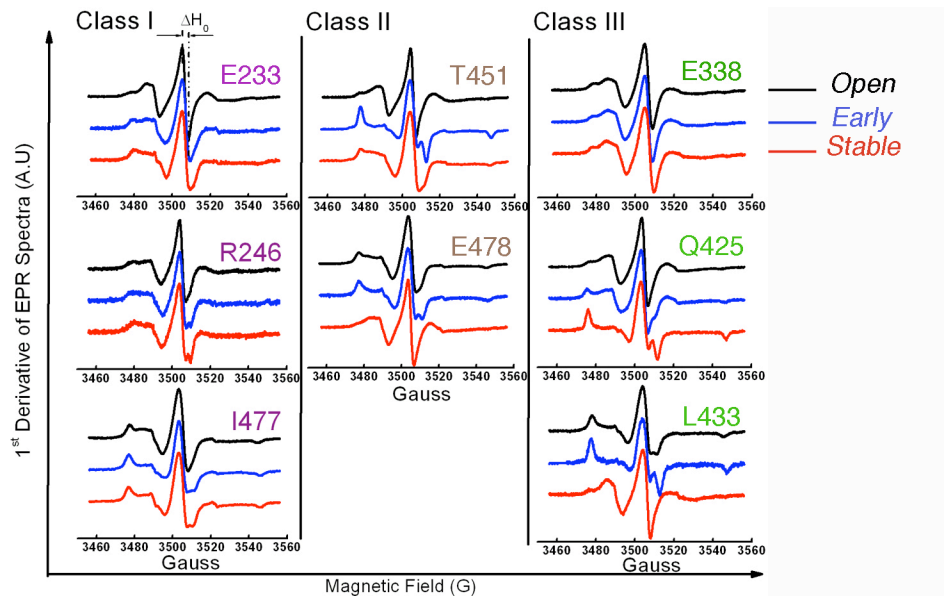


Figure 3.S1. The mobility of residues on SR changed upon formation of early complex (class II), stable complex (class III), or both complexes (class I). The black, blue and red curves represent the free proteins, the early complex and the stable complex, respectively. The mobility of spin-labeled residue was derived from the line width (ΔH_0) of the central resonance and the breadth of the spectra.

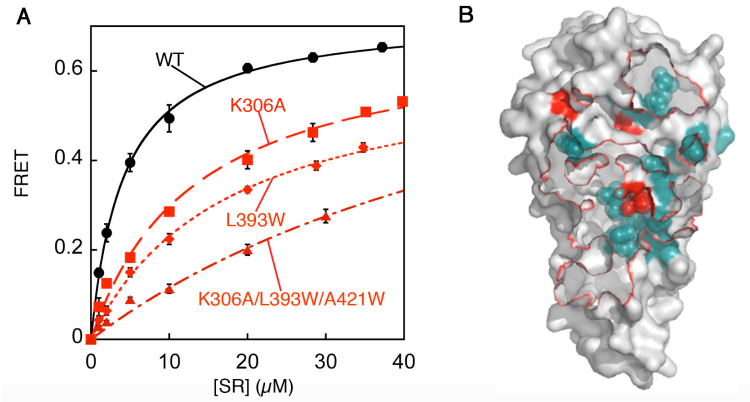


Figure 3.S2. Mutants that disrupt the formation of the stable complex only caused moderate defect in the stability of the early complex. (A) The stability of the early complexes formed by mutants was determined by equilibrium titration experiments. Nonlinear fits gave the equilibrium constants (K_d) of the early complexes as 4.1 μM for wild-type SR, 13.2 μM for SR (K306A), 17.3 μM for SR (L393W), and 31.3 μM for SR (K306A:L393W:A421W). (B) Positions of the SR mutants (cyan) studied in this work are shown on the surface representation of the SR. The three moderately defective mutants are highlighted in red. Red lines on the surface representation denotes the interaction surface between SRP and SR in the stable complex.

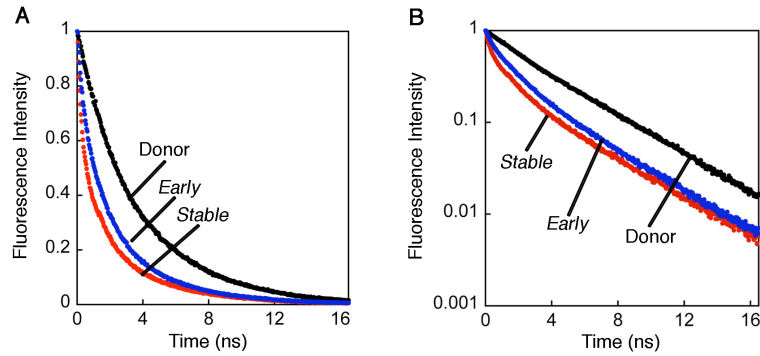


Figure 3.S3. Fluorescence decay of FRET donor (DACM) labeled at SRP (235C) under different experimental conditions. The black, blue, and red curves represent donor-only, donor-acceptor in the early complex, and donor-acceptor in the stable complex, respectively. The fluorescence decay curves in the linear and logarithmic scales are shown in (A) and (B), respectively. Donor-only measurement gave the linear decay of the donor fluorescence and could be fitted to a single exponential decay equation; suggesting that only one decay rate constant was observed. In contrast, the donor-acceptor curves in both the early and stable complexes gave non-linear decay of the donor fluorescence and could be fitted to a multiple-exponential decay equation; suggesting that multiple decay rate constants were recorded.

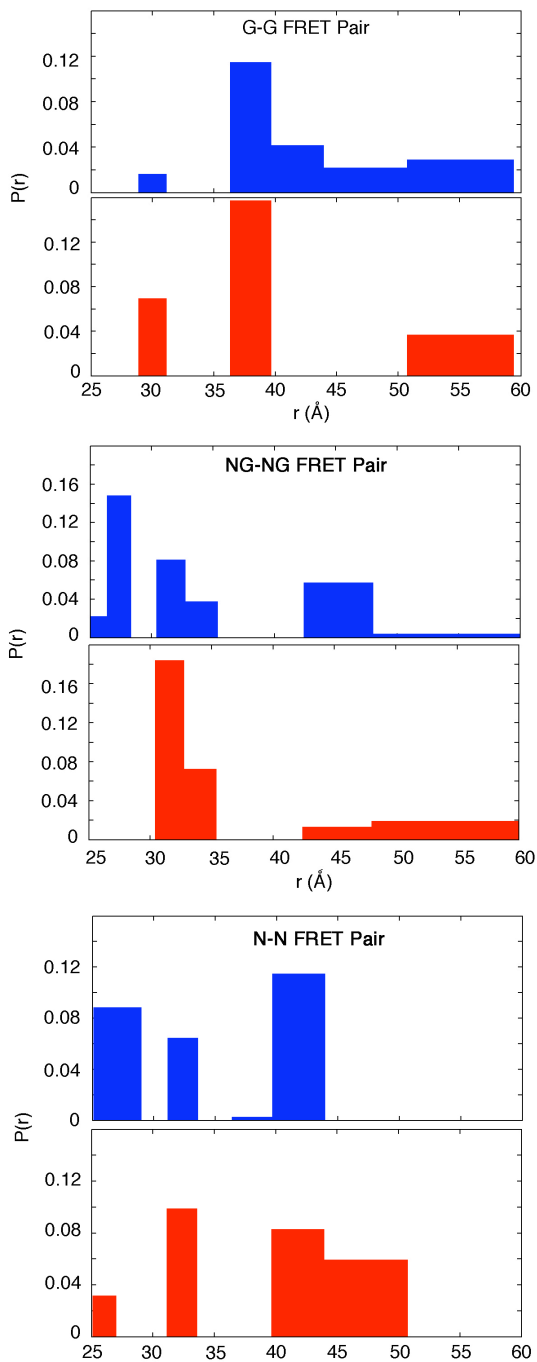


Figure 3.S4. Distance distributions derived from the least-square analyses (LSQ) of the TR-FRET kinetics data. Distribution of $P(r)$ was measured for each FRET pair in the pre-formed early complexes (blue) or stable complexes (red) under equilibrium condition.

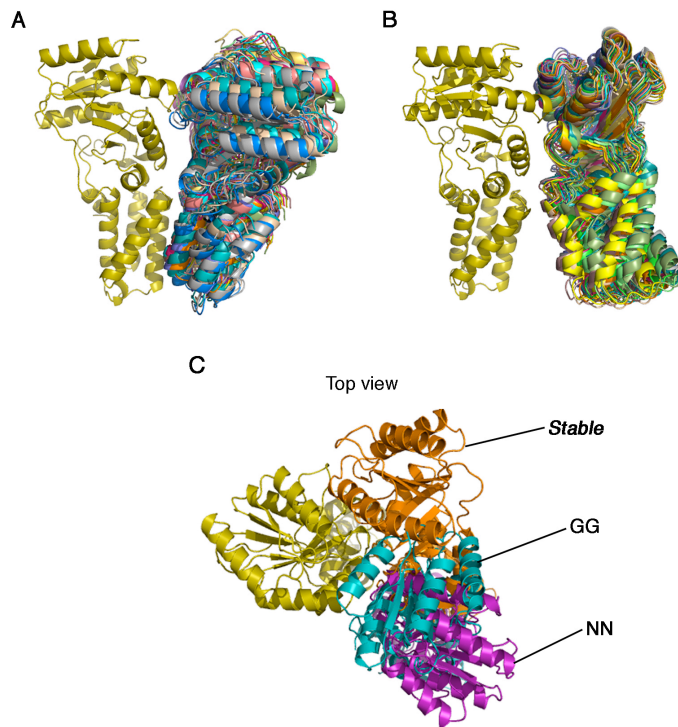


Figure 3.S5. Structural models of the SRP-SR early complex generated by molecular docking. **(A)** and **(B)**: Ensemble of the NN and GG complexes. Structures were overlaid on the top of the SRP GTPase (gold). **(C)**: Top view of the center structures of NN (pink) and GG (cyan) complexes in comparison to that of the co-crystal structure of the stable complex (brown). Structures were overlaid on the top of the SRP GTPase (gold). In the NN conformations, the G domain of the SR GTPase (FtsY) made no contact to the G domain of the SRP GTPase (Ffh). Although the G domains of both GTPases contacted one another in the GG conformations, the interaction surface was not fully formed and the GTP-binding pockets were open to allow free-exchange of nucleotide, explaining why the early complex is GTP-independent. To form the stable complex, extensive conformational rearrangements would be required in the early complex to establish an interaction surface between the SRP and SR GTPases. In particular, the G domains need to undergo a large sliding motion to achieve the correct orientation that is shown in the stable complex.

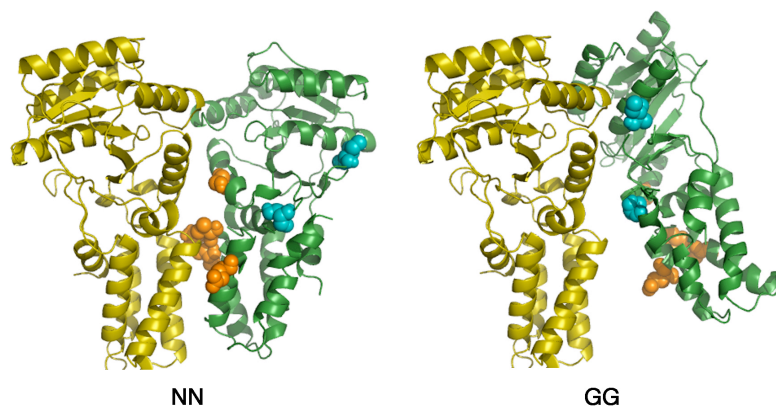


Figure 3.S6. Residues that changed mobility upon formation of the early complex resided close to the interaction surface of either the NN (orange residues) or the GG (cyan residues) complexes.

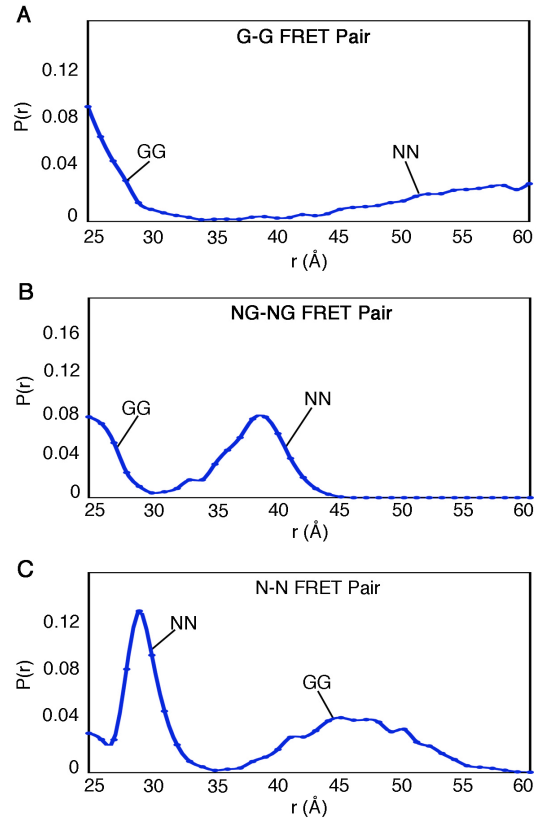


Figure 3.S7. Theoretical distance distributions derived from the NN and GG complexes for all FRET pairs.

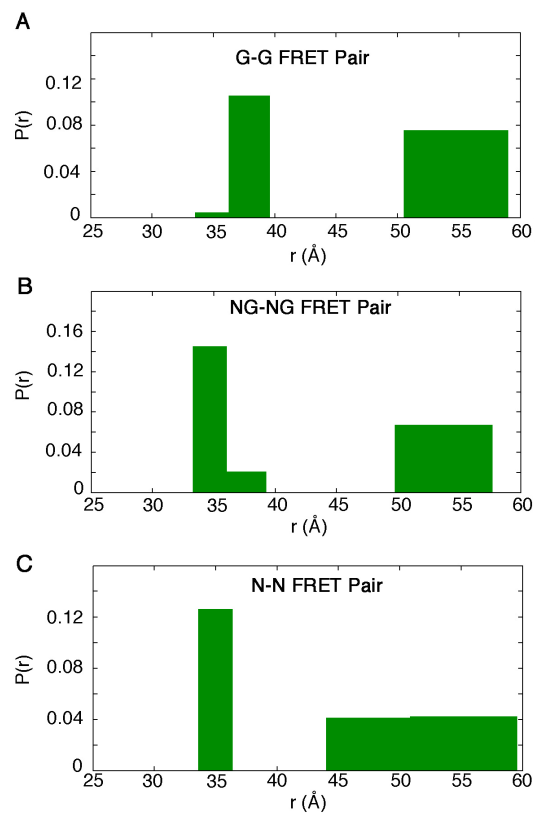


Figure 3.S8. Distance distributions derived from the least-square analyses (LSQ) of the TR-FRET kinetics data. Distribution of $P(r)$ was measured for each FRET pair in the preformed early complexes (green) in the presence of RNC_{FtsQ} .

3.7 Acknowledgements

I thank H. B. Gray for insightful discussions; Vinh Lam and Caltech EPR facility for carrying out EPR measurements; Jaeyoon Chung for protein purification and fluorescence labeling; Tetsunari Kimura and Jay W. Winkler for TR-FRET experiments; Yum Mou and Stephen L. Mayo for molecular docking and Brownian dynamics simulation; and Shan laboratory for helpful suggestions to experimental design. This work was supported by NIH grant GM078024, and career awards from the Burroughs Wellcome Foundation, the Henry and Camille Dreyfus foundation, the Beckman foundation, and the Packard foundation to S. S.